



In utero delivery of targeted ionizable lipid nanoparticles facilitates in vivo gene editing of hematopoietic stem cells

Rohan Palanki^{a,b,1} , John S. Riley^{b,1} , Sourav K. Bose^b , Valerie Luks^b, Apeksha Dave^b, Nicole Kus^b, Brandon M. White^b, Adele S. Ricciardi^{a,b}, Kelsey L. Swingle^a , Lulu Xue^a , Derek Sung^c , Ajay S. Thatte^a, Hannah C. Safford^a , Venkata S. Chaluvadi^d, Marco Carpenter^b , Emily L. Han^a , Rohin Maganti^{a,b}, Alex G. Hamilton^a , Kaitlin Mrksich^a , Margaret B. Billingsley^a , Philip W. Zoltick^b, Mohamad-Gabriel Alameh^e, Drew Weissman^c, Michael J. Mitchell^{a,2} , and William H. Peranteau^{b,2}

Affiliations are included on p. 11.

Edited by Jordan J. Green, Johns Hopkins University, Baltimore, MD; received February 11, 2024; accepted June 28, 2024 by Editorial Board Member Rakesh K. Jain

Monogenic blood diseases are among the most common genetic disorders worldwide. These diseases result in significant pediatric and adult morbidity, and some can result in death prior to birth. Novel ex vivo hematopoietic stem cell (HSC) gene editing therapies hold tremendous promise to alter the therapeutic landscape but are not without potential limitations. In vivo gene editing therapies offer a potentially safer and more accessible treatment for these diseases but are hindered by a lack of delivery vectors targeting HSCs, which reside in the difficult-to-access bone marrow niche. Here, we propose that this biological barrier can be overcome by taking advantage of HSC residence in the easily accessible liver during fetal development. To facilitate the delivery of gene editing cargo to fetal HSCs, we developed an ionizable lipid nanoparticle (LNP) platform targeting the CD45 receptor on the surface of HSCs. After validating that targeted LNPs improved messenger ribonucleic acid (mRNA) delivery to hematopoietic lineage cells via a CD45-specific mechanism in vitro, we demonstrated that this platform mediated safe, potent, and long-term gene modulation of HSCs in vivo in multiple mouse models. We further optimized this LNP platform in vitro to encapsulate and deliver CRISPR-based nucleic acid cargos. Finally, we showed that optimized and targeted LNPs enhanced gene editing at a proof-of-concept locus in fetal HSCs after a single in utero intravenous injection. By targeting HSCs in vivo during fetal development, our Systematically optimized Targeted Editing Machinery (STEM) LNPs may provide a translatable strategy to treat monogenic blood diseases before birth.

lipid nanoparticles | mRNA | hematopoietic stem cell | CRISPR | congenital disease

Monogenic blood diseases, including sickle cell disease and α/β thalassemia, are among the most common genetic disorders worldwide (1). These diseases result in significant pediatric morbidity, including painful vaso-occlusive crises, severe anemia, increased susceptibility to life-threatening infections, and, in some cases, fetal demise (2, 3). mRNA-based therapeutics targeting hematopoietic stem cells (HSCs) hold great promise for the treatment of these diseases by producing missing or defective blood proteins, correcting specific disease-causing genetic variants, or up-regulating compensatory globins via gene editing (4, 5).

Recent advances in clustered regularly interspaced short palindromic repeat (CRISPR)-based gene editing technology and ex vivo gene delivery to HSCs have enabled United States Food and Drug Administration (FDA) approval of autologous HSC-based gene therapies for the treatment of sickle cell disease and β thalassemia (6). These first-in-kind therapies rely on physical or viral methods for gene replacement or gene editing of patient-derived CD34⁺ HSCs (7). Modified cells are then transplanted back into patients pre-treated with myeloablative conditioning. While clinical outcomes for these treatments are promising, ex vivo HSC gene therapy is an expensive (\$2-3 million per dose) and time-consuming (months-long) process, requiring a specialized cell processing center and extensive clinical transplantation expertise (8). In addition, the chemotherapy required to reach clinically relevant HSC engraftment levels can be neurotoxic and may result in prolonged hospital stays (9, 10). Importantly, the resource and infrastructure requirements for these novel gene therapies limit their utility in low- and middle-income countries, where the majority of monogenic blood disease burden exists (11).

In contrast, in vivo gene editing for monogenic blood diseases offers a more facile and potentially lower cost treatment paradigm without a need for HSC collection, ex vivo culture, preconditioning, or transplant (8, 12). HSCs may be modified directly within

Significance

In vivo mRNA delivery to hematopoietic stem cells (HSCs) in the bone marrow is a significant barrier to engineering in vivo gene editing therapies for monogenic blood diseases. During fetal development, HSCs reside in the liver, where they are more accessible. To facilitate the delivery of gene editing cargo to fetal HSCs, we designed and optimized an ionizable lipid nanoparticle (LNP) platform targeted to the CD45 receptor expressed on the surface of HSCs. CD45 receptor-targeted LNPs administered via a single in utero intravenous injection mediated safe, potent, and durable gene editing of HSCs in vivo in mice. Our delivery strategy unlocks the possibility to treat monogenic blood diseases in utero prior to the onset of irreversible pathogenesis.

Competing interest statement: R.P., M.J.M., and W.H.P. are inventors on a U.S. Provisional Patent Application (No. 63/623,674) related to the technology described in the manuscript.

This article is a PNAS Direct Submission. J.J.G. is a guest editor invited by the Editorial Board.

Copyright © 2024 the Author(s). Published by PNAS. This article is distributed under [Creative Commons Attribution-NonCommercial-NoDerivatives License 4.0 \(CC BY-NC-ND\)](https://creativecommons.org/licenses/by-nc-nd/4.0/).

¹R.P. and J.S.R. contributed equally to this work.

²To whom correspondence may be addressed. Email: mjmitch@seas.upenn.edu or peranteauw@chop.edu.

This article contains supporting information online at <https://www.pnas.org/lookup/suppl/doi:10.1073/pnas.2400783121/-/DCSupplemental>.

Published July 30, 2024.

their niche in vivo after intravenous (IV) administration of a therapy in an outpatient center. An in vivo approach also unlocks the possibility to treat a disease in utero prior to the onset of disease pathogenesis (4, 13). This is especially relevant for diseases like α thalassemia major that carry an elevated risk of fetal mortality (3). The clinical translation of in vivo gene therapies, including gene editing therapies, for monogenic blood diseases has been hindered by a limited number of effective and nontoxic platforms designed to facilitate gene delivery to HSCs. For example, adenoviral vectors have been designed for in vivo modification of HSCs (14, 15); however, viral delivery platforms may have toxicity and immunogenicity concerns at high doses (16). Nonviral delivery carriers, such as ionizable lipid nanoparticles (LNPs), have demonstrated clinical success for in vivo vaccine and liver disease applications (17), yet extrahepatic tropism and efficacy require significant optimization (18). While others have developed LNPs targeting HSCs in vivo (19, 20), these studies are limited by the delivery of reporter or gene modifying cargos and assessment in adult mouse models, when disease processes may have already matured.

Taking advantage of HSC residence in the liver during fetal development (21), here we engineer an LNP platform to facilitate in vivo gene editing of fetal HSCs and their progeny (Fig. 1A). Specifically, we propose that HSCs—after modification via engineered LNPs in utero—will carry forth a designated therapeutic edit upon physiologic migration into the bone marrow, thereby mitigating disease long-term in the hematopoietic niche and circulating blood supply. To target fetal HSCs in vivo, CD45 antibody-conjugated LNPs carrying mRNA encoding genome modifying or gene editing cargos were designed, optimized, and tested in multiple mouse models. Targeted LNPs exhibited safe, durable, and potent gene editing of fetal HSCs in mice after a single IV injection, offering proof-of-concept evidence for the use of this delivery strategy to treat monogenic blood disease in utero.

Results

Baseline LNP-Mediated Transfection of Mouse HSCs In Utero.

LNPs are conventionally formulated with four organic components: an ionizable lipid for nucleic acid loading and endosomal escape of nucleic acid cargo, phospholipid for bilayer stability, cholesterol for membrane rigidity, and lipid-anchored polyethylene glycol (PEG) for reduced aggregation and increased circulation time (22). A major advantage of LNPs for gene delivery applications is their modularity. Organic excipients can be interchanged to produce LNPs with distinct physiochemical properties, passively shifting biodistribution toward specific organs or cell types (23, 24). Alternatively, target-specific ligands can be included during LNP formulation to actively influence tissue or cellular tropism (25). In this study, we sought to maximize LNP transfection of HSCs in vivo.

We previously identified a potent ionizable lipid (i.e., C14-490) for transfection of the mouse fetal liver following in utero IV injection at gestational day (E) 16 (26). Here, we studied the biodistribution of C14-490 LNPs at E13.5, a timepoint when hematopoiesis is known to occur predominantly in the liver (21). R26^{mT/mG} fetuses (dual-fluorescent floxed reporter mouse model) were injected at E13.5 with either phosphate-buffered saline (PBS) or C14-490 LNPs encapsulating Cre mRNA at a dose of 1 mg/kg mRNA. After 60 h, fetal tissues were harvested, demonstrating transfection of the whole fetus (SI Appendix, Fig. S1A) and fetal liver (SI Appendix, Fig. S1B). While 50% of fetal hepatocytes were transfected (SI Appendix, Fig. S1C), only 2% of fetal HSCs (Lin-/Sca1+/cKit+) were transfected, demonstrating that passive biodistribution alone was insufficient for robust LNP delivery to HSCs at this developmental stage.

Design and Characterization of Anti-CD45 LNPs. To enhance LNP-mediated transfection of HSCs, we utilized an active targeting approach leveraging the CD45 receptor (CD45R), a type 1 transmembrane protein tyrosine phosphatase expressed on the surface of HSCs (Fig. 1B and C) (27). To specifically engage the CD45R, CD45 antibody F(ab')₂ fragments were conjugated to the surface of C14-490 LNPs composed of a 5:1 ratio of PEG to PEG-maleimide via a thiol-maleimide reaction (targeted LNPs). C14-490 LNPs possessing PEG-maleimide moieties but without CD45 antibody functionalization (untargeted LNPs) served as controls. For initial studies, both targeted and untargeted LNPs were formulated to encapsulate reporter green fluorescent protein (GFP) mRNA. Targeted LNPs displayed a ~20 nm increase in average diameter relative to untargeted LNPs (Fig. 1D) without aggregation (Fig. 1E) and with excellent mRNA encapsulation efficiency (Fig. 1F).

We tested the impact of CD45 antibody conjugation to LNPs on the resultant transfection efficacy of Jurkat cells, an immortalized human T cell line, in vitro. Importantly, 100% of untreated Jurkat cells constitutively express the CD45R on their surface (SI Appendix, Fig. S2). Jurkat cells were treated with either targeted or untargeted LNP encapsulating GFP mRNA and assessed for downstream GFP fluorescence via flow cytometry after 24 h. Targeted LNPs facilitated an eightfold improvement in functional mRNA delivery to Jurkat cells relative to untargeted LNPs (Fig. 2A) without in vitro cytotoxicity (Fig. 2B). Enhancement in mRNA delivery was also shown to be dose-dependent (Fig. 2C). Targeted LNPs formulated with a 5:1 ratio of PEG to PEG-maleimide maximized mRNA delivery to Jurkat cells relative to lower (7:1 ratio) and higher ratios (3:1) of the linker group (SI Appendix, Fig. S3). Since our eventual goal was to develop a targeted LNP that enhances in vivo human HSC transfection, particularly in fetal recipients, we next evaluated the efficacy of GFP mRNA delivery via targeted LNPs to CD34+ primary human cord blood cells (SI Appendix, Fig. S4) and CD34+ human fetal liver progenitor cells (SI Appendix, Fig. S5). These studies demonstrated enhanced GFP expression—threefold in cord blood cells and fivefold in fetal liver cells—when reporter mRNA was delivered via targeted LNPs. Together, these results validated our active targeting strategy, demonstrating that LNP conjugation to CD45 antibody fragments improves transfection of immune cells possessing the cognate receptor.

We next tested the specificity of targeted LNP efficacy to CD45 antibody functionalization. Targeted LNPs conjugated to IgG isotype control antibody fragments (IgG LNPs) were generated using the same method. IgG LNPs facilitated a similar level of transfection to untargeted LNPs in Jurkat cells (Fig. 2D) despite having similar physiochemical properties to targeted LNPs (SI Appendix, Fig. S6). To determine whether CD45-CD45R interactions facilitated improvement in mRNA delivery, Jurkat cells were pre-treated with free CD45 antibodies prior to untargeted or targeted LNP treatment. As the dose of free CD45 antibody pre-treatment increased, reporter mRNA delivery via targeted LNPs diminished (Fig. 2E). A similar experiment was conducted with pre-treatment of free IgG isotype control antibodies, yet a corresponding reduction in targeted LNP transfection was not observed, suggesting that the enhanced efficacy of targeted LNPs was CD45 specific (Fig. 2F). To further assess the specificity of LNPs functionalized with CD45 antibodies, we performed additional experiments using HepG2 cells which do not express CD45R. In these cells, there was no increase in cell transfection with the addition of CD45 targeting moieties to the surface of LNPs (Fig. 2G).

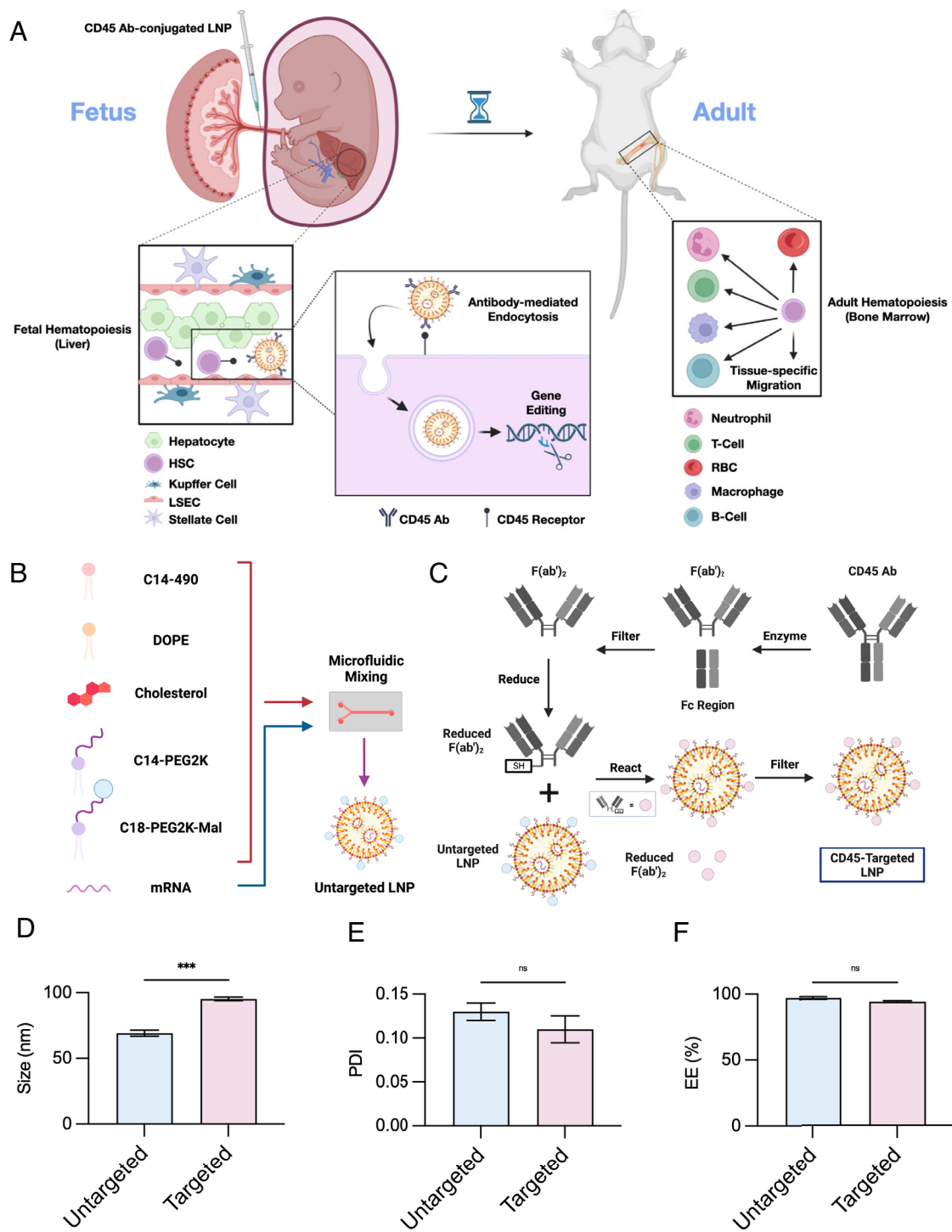


Fig. 1. Design and characterization of CD45R-targeted LNPs. (A) Schematic describing the overall experimental rationale for this study. In brief, LNPs conjugated to CD45 antibody fragments will hone to CD45 receptors expressed on the surface of HSCs within the fetal mouse liver microenvironment. Following LNP internalization in utero and nucleic acid cargo-mediated modification, gene-edited HSCs will undergo normal physiological migration to the bone marrow, where they will engraft and coordinate hematopoiesis of myeloid and lymphoid progeny that also possess the progenitor cell edit. (B) Untargeted LNP formulation scheme that involves C14-490 ionizable lipid, DOPE, cholesterol, C14-PEG2K, and a C18-PEG2K-maleimide (mal-PEG) linker in the organic phase mixed via a microfluidic device with designated RNA cargo in citric acid buffer. (C) Schematic visualizing CD45 F(ab)₂ antibody generation and conjugation to untargeted LNPs to generate targeted LNPs. (D) Characterizing the size, (E) polydispersity (PDI), and (F) encapsulation efficiency of untargeted LNPs (blue) and targeted LNPs (pink). Unpaired parametric Student's *t* test ($P < 0.05$) was used to compare the physicochemical properties of untargeted and targeted LNPs (ns = non-significant, *** $P < 0.001$); all data reported as the mean \pm SEM (minimum $n = 3$).

Finally, we sought to determine whether the addition of CD45 antibodies to the surface of LNPs significantly altered the LNP protein corona. We utilized unbiased mass spectrometry-based proteomics to identify the plasma proteins that bind the surface of untargeted or targeted LNPs ex vivo. We found that among the

859 distinct proteins adsorbed to the surface of both untargeted and targeted LNPs, 94% of these proteins were not differentially abundant between groups (Fig. 2*H*). The impact of the LNP protein corona was then investigated in Jurkat cells treated with untargeted or targeted LNPs pre-incubated in either plasma or PBS.

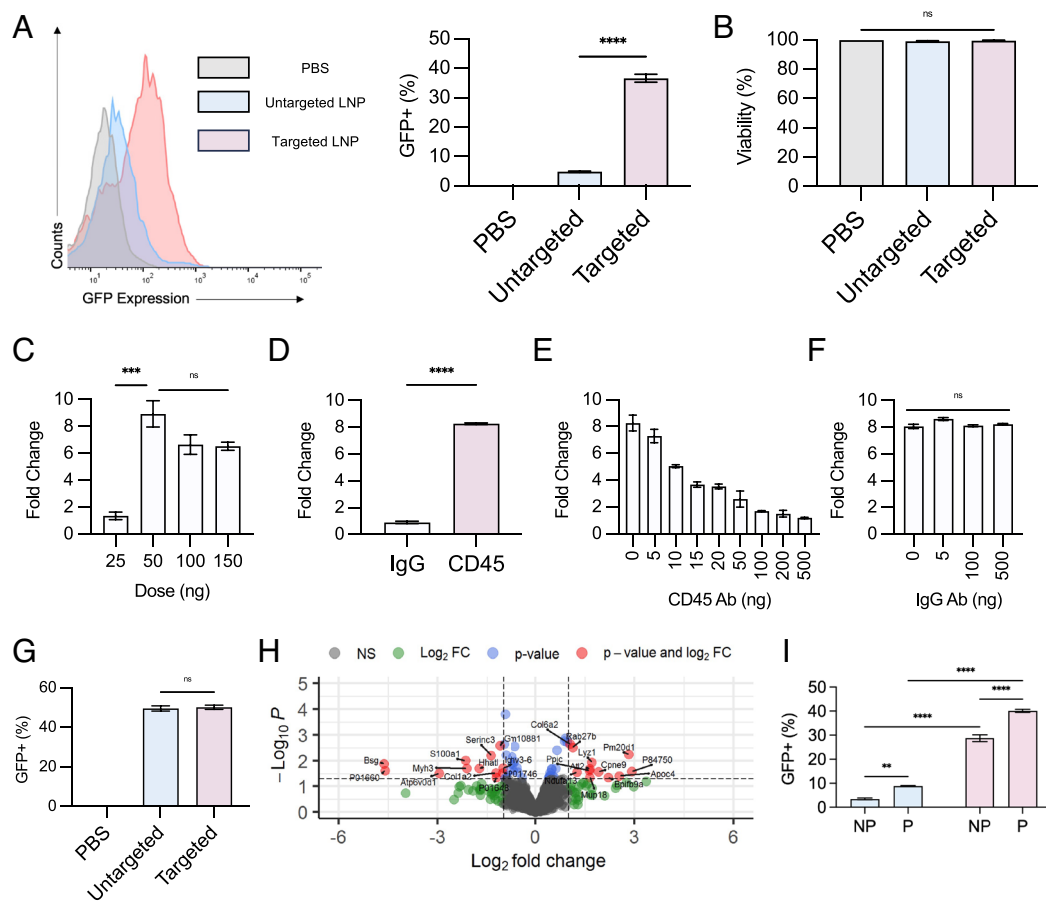


Fig. 2. Investigating the efficacy, safety, and mechanism of CD45R-targeted LNPs. (A) Percentage of Jurkat cells (CD45+) expressing GFP 24 h after treatment with untargeted LNPs (blue) or targeted LNPs (pink) encapsulating GFP mRNA at a dose of 100 ng/30,000 cells, visualized via histogram (Left) and plotted (Right). PBS treatment (gray) was used as a negative control. (B) Viability of Jurkat cells following treatment used in (A). (C) Effect of dose (per 30,000 cells) on fold improvement in mRNA delivery to Jurkat (targeted LNP/untargeted LNP). (D) Effect of antibody substitution (CD45 → IgG isotype control) on targeted LNP efficacy in mRNA delivery to Jurkat. (E) Effect of CD45 antibody or (F) IgG antibody pre-treatment on the fold improvement in mRNA delivery to Jurkat (targeted LNP/untargeted LNP). (G) Percentage of HepG2 cells (CD45-) expressing GFP 24 h after treatment with untargeted LNPs or targeted LNPs encapsulating GFP mRNA at a dose of 25 ng/30,000 cells. (H) Volcano plot summarizing the differentially abundant proteins within the corona of plasma-incubated untargeted LNPs and targeted LNPs. (I) Percentage of Jurkat cells expressing GFP after treatment via the approach used in (A) with (P) or without (NP) pre-incubation in plasma. One-way ANOVA with post hoc Dunnett's test was used to compare the effect of untargeted LNP or targeted LNP treatment in vitro (A–C, F, G, and I). Unpaired parametric Student's *t* test ($P < 0.05$) was used to compare the efficacy of CD45 and IgG-targeted LNPs (D) (ns = non-significant, * $P < 0.05$, ** $P < 0.01$, *** $P < 0.001$, **** $P < 0.0001$); all data reported as the mean \pm SEM (minimum $n = 3$).

Although pre-incubation in plasma resulted in a minor improvement in mRNA delivery for both untargeted and targeted LNPs, CD45 functionalization played a greater role in mediating cell transfection in both groups (Fig. 2J). In sum, these results supported that targeted LNPs utilize a CD45R-specific mechanism to improve transfection of hematopoietic lineage cells in vitro.

Targeted LNPs Enhance mRNA Delivery to HSCs In Utero. We next evaluated the safety and efficacy of targeted LNPs in vivo. R26^{mT/mG} fetuses were injected at E13.5 with untargeted or targeted LNPs encapsulating Cre mRNA at a dose of 1 mg/kg mRNA. After 60 h, fetal livers were harvested and processed for fetal hepatocytes and fetal HSCs. Both untargeted and targeted LNPs transfected ~50% of fetal hepatocytes (Fig. 3A). While only 4% of fetal HSCs were transfected after untargeted LNP administration, 30% of fetal HSCs were transfected after targeted LNP administration (Fig. 3A). Transfection of CD45+ cells in the fetal liver by targeted LNPs was confirmed on histology (Fig. 3B). Interestingly, when a similar experiment was conducted in adult R26^{mT/mG} mice, both untargeted and targeted LNPs resulted in strong transfection of the liver but failed to produce discernable genome modulation in adult bone marrow HSCs (Fig. 3C). These results imply that transfection

of HSCs via this strategy requires both active targeting to HSCs and the fetal microenvironment, which possesses an accessible and abundant population of these cells.

The durability of genome modulation via this approach was subsequently assessed in vivo. Of note, Cre recombinase-mediated excision of the LoxP flanked tdTomato cassette in R26^{mT/mG} mice results in permanent expression of green fluorescence protein in transfected cells and their progeny. Thus, we injected R26^{mT/mG} fetuses at E13.5 with untargeted or targeted LNPs encapsulating Cre mRNA at a dose of 1 mg/kg mRNA and harvested liver, bone marrow, and peripheral blood after 4 mo, when these mice had reached adulthood. In concordance with our results at 60 h, both untargeted and targeted LNPs facilitated long-term transfection in 50% of hepatocytes (Fig. 3C). Targeted LNPs mediated long-term genome modulation in 19% of bone marrow HSCs compared to only 4% of bone marrow HSCs in animals treated with untargeted LNPs (Fig. 3D). Genome modification of hematopoietic lineage cells, including T cells, B cells, monocytes, granulocytes, and erythrocytes, in experimental animals corresponded directly to progenitor HSC transfection in both LNP treatment groups (Fig. 3E). Therefore, not only are targeted LNPs able to facilitate potent and long-term genome modulation in HSCs relative to untargeted

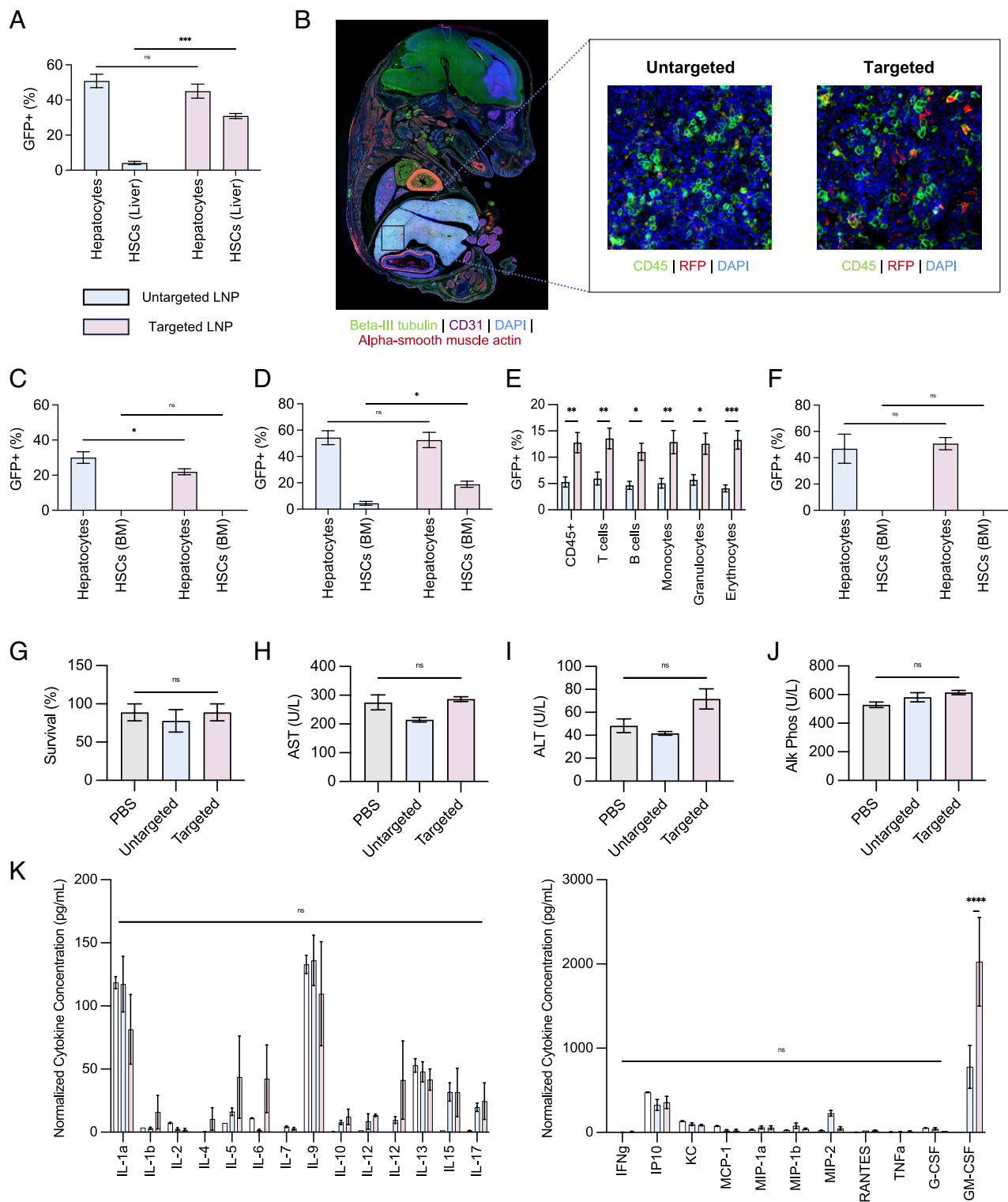


Fig. 3. Efficacy and safety of targeted LNPs in utero. (A) Percentage of hepatocytes (CD45⁻/CD31⁻) or HSCs (Lin⁻/Sca1⁺/cKit⁺) expressing GFP, 60 h after E13.5 R26^{mt/mG} fetal mice were treated with either untargeted LNPs (blue) or targeted LNPs (pink) encapsulating Cre mRNA at a dose of 1 mg/kg. (B) Histological representation of an E14.5 Balb/c mouse fetus (*Left*) and corresponding fetal livers (*Right*) from mice treated via in utero IV injection with untargeted LNPs or targeted LNPs encapsulating mCherry mRNA at a dose of 1 mg/kg. Colocalization of CD45 (green) and RFP (red) indicates delivery to CD45⁺ cells. (C) Percentage of GFP⁺ hepatocytes and HSCs, 60 h after 12-wk-old adult R26^{mt/mG} mice were treated as described in (A). (D) Percentage of GFP⁺ hepatocytes and bone marrow HSCs, 4 mo after E13.5 R26^{mt/mG} fetal mice were treated as described in (A). (E) Percentage of myeloid or lymphoid cells in recipient mice expressing GFP at terminal harvest of R26^{mt/mG} mice treated in utero. (F) Percentage of GFP⁺ hepatocytes and bone marrow HSCs, 4 mo after 12-wk-old adult R26^{mt/mG} mice were treated as described in (A). (G) R26^{mt/mG} fetus survival to birth following in utero IV injection of PBS, untargeted LNPs, or targeted LNPs. (H) Serum aspartate transaminase (AST), (I) alanine transaminase, (J) alkaline phosphatase, and (K) serum cytokine levels of R26^{mt/mG} fetal mice treated at E13.5 with PBS, untargeted LNPs, or targeted LNPs and harvested after 24 h. One-way ANOVA with post hoc Dunnett's test was used to compare efficacy (A, C, D, and F) and safety (G, H, I, and J) of untargeted and targeted LNPs. Two-way ANOVA with post hoc Sidák's multiple comparisons test was used to compare the effect of untargeted and targeted LNP treatment on multilineage hematopoietic cell transfection (E) and induction of acute cytokine response (K) (ns = non-significant, **P* < 0.05, ***P* < 0.01, ****P* < 0.001, *****P* < 0.0001); all data reported as the mean ± SEM (minimum n = 3).

LNPs, but these LNP-mediated edits are passed down proportionally to cell progeny within the peripheral blood. As expected, long-term genome modification after 4 mo was not observed in a similar cohort of R26^{mT/mG} mice treated as adults with either untargeted or targeted LNPs (Fig. 3F).

Given the high ethical standards for fetal intervention, we characterized the safety of this delivery strategy in vivo. First, in our long-term cohort of R26^{mT/mG} mice injected at E13.5, survival to birth was equivalent between PBS-, untargeted LNP-, and targeted LNP-treated fetuses (Fig. 3G). Next, we assessed liver enzyme and cytokine levels 24 h after in utero IV administration of either PBS, untargeted LNPs, or targeted LNPs in wild-type mice. AST, ALT, and alkaline phosphatase levels were found to be similar in targeted LNP-treated mice relative to PBS-treated controls (Fig. 3H, I, and J). Further analysis of fetal blood revealed that 24 out of 25 cytokines measured were not significantly elevated in LNP-treated mice relative to PBS-treated controls (Fig. 3K). GM-CSF (a regulator of macrophage production) was increased in both LNP treatment groups, as we observed previously following LNP administration (28). However, levels of this acute phase cytokine returned to normal in LNP-treated mice after 48 h (SI Appendix, Fig. S7). Although additional studies are warranted to fully characterize the safety of targeted LNPs, the limited toxicity observed confirmed the potential suitability of this platform for downstream fetal HSC gene editing applications.

Secondary Transplant Confirms Targeted LNP-Mediated Transfection of Mouse LT-HSCs. While genome modification of hematopoietic lineage cells 4 mo following in utero LNP administration supports transfection of a self-renewing HSC population, we sought to further confirm that targeted LNPs were truly delivering the mRNA cargo to a long-term population of HSCs (LT-HSCs). The gold standard definition of a LT-HSC is a cell that when transferred

into an irradiated recipient will have the ability to reestablish blood cell production long-term in the recipient (29). To definitively confirm that targeted LNPs transfect multipotent and self-renewing mouse LT-HSCs, we conducted a secondary transplant study using R26^{mT/mG} and wild-type mice (Fig. 4A). R26^{mT/mG} mice were injected at E13.5 with targeted LNPs encapsulating Cre mRNA at a dose of 1 mg/kg prior to bone marrow harvest at 4 mo of age (donors). A separate cohort of adult wild-type mice underwent total body irradiation (10.4 Gy, split across two doses) to eliminate the native hematopoietic niche (recipients). Donor whole bone marrow (WBM)—at an initial transfection rate of 20%—was then transplanted into recipient mice via IV injection, and recipients were followed for 4 mo via peripheral blood draws before terminal bone marrow harvest. Of note, recipient mice had no prior exposure to LNP treatment and minimal background signal. Thus, observed green fluorescence could be attributed to secondary transplant from donor mice.

Analysis of peripheral blood 1 mo after secondary transplant revealed that 20% of hematopoietic lineage cells (CD45+) in recipient mice expressed GFP, matching the initial transfection efficiency of transplanted cells (Fig. 4B). GFP expression in this population of cells was maintained over the course of 4 mo (Fig. 4B), and 100% of mice survived to terminal harvest. At terminal harvest, nearly 20% of hematopoietic lineage cells in the recipient peripheral blood, including T cells, B cells, monocytes, granulocytes, and erythrocytes, expressed GFP, possessing the same efficiency of genome modification as transplanted cells (Fig. 4C). In addition, 4 mo after secondary transplantation, approximately 25% of HSCs in the bone marrow of recipient mice expressed GFP, suggesting that these engrafted cells originated from transplanted progenitor LT-HSCs (Fig. 4D). Together, these results provide strong evidence that administration of targeted LNPs in utero facilitates durable and definitive in vivo genome modulation in mouse LT-HSCs.

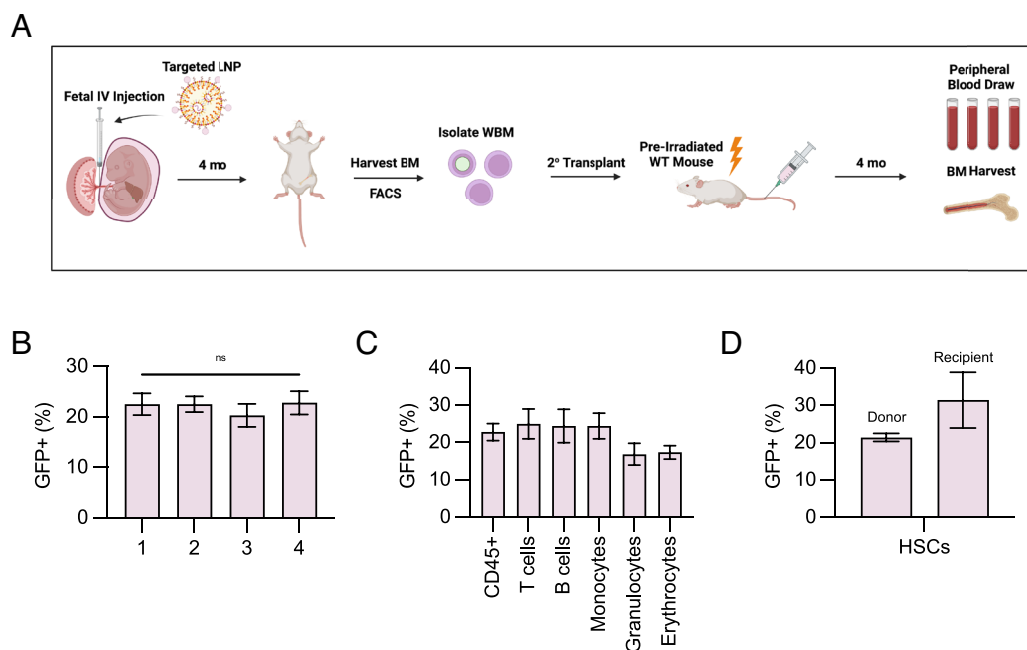


Fig. 4. Secondary transplant of HSCs modified via targeted LNPs in utero. (A) Schematic of secondary transplant study. E13.5 R26^{mT/mG} fetuses were treated with targeted LNPs encapsulating Cre mRNA via in utero IV injection at a dose of 1 mg/kg and followed for 4 mo prior to WBM isolation (donors) and secondary transplanted into lethally irradiated wild-type adult mice (recipients). Recipient mice were subsequently followed for 4 mo via peripheral blood draw prior to terminal BM harvest and assessment of gene modulation in engrafted HSCs. (B) Percentage of CD45+ cells in recipient mice expressing GFP at a given month following secondary transplant. (C) Percentage of myeloid or lymphoid cells in recipient mice expressing GFP at terminal harvest after 4 mo. (D) Percentage of HSCs (Lin⁻/Sca1⁺/cKit⁺) expressing GFP within the bone marrow of donor mice (4 mo after treatment in utero with targeted LNPs) and the bone marrow of recipient mice (4 mo after secondary transplant). One-way ANOVA with post hoc Dunnett's test was used to compare the level of GFP positivity in recipient mouse CD45+ cells over time (B) (ns = non-significant); all data reported as the mean ± SEM (minimum n = 3).

Design of Experiments (DOE) Reveals Optimal LNP Formulation for Delivery of Gene Editing Cargo. Codelivery of Cas9 mRNA and a single guide RNA (sgRNA) is a promising strategy for therapeutic genome editing in a range of cells, including HSCs. However, delivery of large mRNA cargos such as these via LNPs remains a significant engineering challenge (30). One strategy to maximize LNP-mediated mRNA delivery involves optimization of organic excipient molar ratios (23, 24, 31), which can be evaluated in a high-throughput manner via orthogonal DOE.

Thus, we used principles of DOE to design and formulate sequential libraries of C14-490 LNPs encapsulating *Streptococcus pyogenes* Cas9 (SpCas9) mRNA and an sgRNA designed to knock-out GFP (GFP sgRNA) with varied excipient molar ratios (Fig. 5A). LNPs from these libraries were screened in vitro in HepG2 cells constitutively expressing GFP (HepG2-GFP). Gene editing in this model was quantified via knockout of GFP expression. The first library of C14-490 LNPs (Library A) was characterized for standard physiochemical parameters, including size, PDI, and encapsulation efficiency (SI Appendix, Figs. S8 and S9). The 16 LNPs in Library A and the initial LNP formulation (A0) were then screened in HepG2-GFP cells. Relative to the initial A0 formulation of C14-490 LNPs, 3 LNPs (A1, A11, A14) facilitated greater gene editing (Fig. 5B). We also observed that LNP-mediated gene editing was higher with increasing molar fraction of ionizable lipid and

decreasing molar fraction of phospholipid, cholesterol, and PEG within C14-490 LNP formulations (SI Appendix, Fig. S10).

These trends were used to design a second-generation library of C14-490 LNPs (Library B), which was formulated, characterized (SI Appendix, Figs. S8 and S9), and screened in the same in vitro model. Relative to A0 LNPs, 7 LNPs (B1, B2, B3, B4, B5, B7, B9) improved gene editing (Fig. 5C). The top-performing LNP formulations (B1 and B5) enhanced gene editing by 2.5-fold, resulting in gene disruption in approximately 30% of HepG2-GFP cells at a low dose. B5 LNPs were selected for further study based on superior physiochemical properties, including encapsulation efficiency (96.5% vs. 85.4%) and PDI (0.10 vs. 0.24). Given an intended application for hematopoietic disorders, B5 LNPs and A0 LNPs were then evaluated for gene editing efficacy in a GFP-positive hematopoietic lineage cell line (Jurkat-GFP). B5 LNPs enhanced gene editing in Jurkat-GFP cells relative to A0 LNPs by eightfold (Fig. 5D). Thus, sequential rounds of DOE identified a formulation of C14-490 LNPs that was optimized for delivery of gene editing mRNA cargo.

STEM LNPs Facilitate In Utero Gene Editing of Mouse HSCs. We

next tested the gene editing efficacy of unoptimized (A0) and optimized (B5) C14-490 LNPs in vivo. For proof-of-concept studies, we formulated A0 and B5 LNPs encapsulating SpCas9

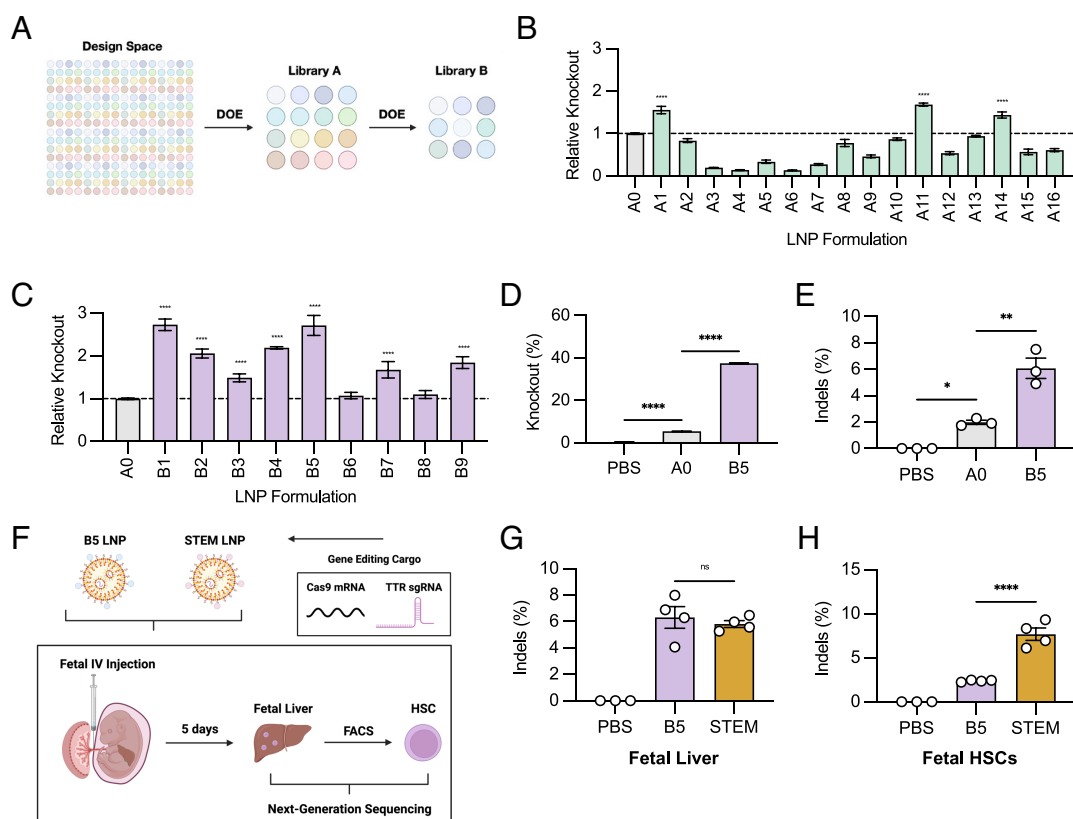


Fig. 5. Optimization and delivery of gene editing cargo to HSCs in utero. (A) Schematic of DOE approach depicting the design space ($4 \times 4 \times 4$) and sequential library generation (Library A \rightarrow Library B). (B) Screening LNPs from Library A encapsulating Cas9 mRNA and GFP sgRNA in HepG2-GFP cells at a dose of 100 ng/30,000 cells. Flow cytometry was used to capture resultant GFP knockout after 5 d. Data normalized to the standard formulation (A0, dotted line). (C) Screening LNPs from Library B via the same approach used in (B). (D) Cross-validating B5 LNP formulation encapsulating Cas9 mRNA and GFP sgRNA in Jurkat-GFP (hematopoietic lineage cells) at a dose of 100 ng/30,000 cells. Flow cytometry was used to capture resultant GFP knockout after 5 d. (E) Testing the gene editing efficacy of unoptimized (A0) and optimized (B5) LNPs encapsulating Cas9 mRNA and TTR sgRNA after in utero IV administration at a dose of 1 mg/kg into E13.5 wild-type mice. Genomic DNA from the fetal liver was harvested after 5 d, and indels at the intended locus were quantified via NGS. PBS-injected fetuses were used as a negative control. (F) Schematic of experiment evaluating the gene editing efficacy of optimized untargeted LNPs (B5) and optimized targeted LNPs (STEM) via the same approach used in (E), although HSCs (Lin⁻/Sca1⁺/cKit⁺) were also isolated and sequenced. (G) Indels at the intended locus in genomic DNA from the fetal liver of animals treated with PBS, B5 LNPs, or STEM LNPs. (H) Indels at the intended locus in genomic DNA from HSCs of animals treated with PBS, B5 LNPs, or STEM LNPs. One-way ANOVA with post hoc Dunnett's test was used to compare gene editing efficacy of LNP formulations (B-E, G, and H) (ns = non-significant, * $P < 0.05$, ** $P < 0.01$, *** $P < 0.001$, **** $P < 0.0001$); all data reported as the mean \pm SEM (minimum $n = 3$).

mRNA and sgRNA specific for the transthyretin (*TTR*) gene (TTR sgRNA). This therapeutic locus is currently being investigated in clinical trials for patients with hereditary transthyretin amyloidosis (32). Knockout of the *TTR* gene leads to reduction of misfolded TTR protein and subsequently prevents buildup of pathogenic amyloid plaques. Given that the liver is the almost exclusive depot of TTR protein manufacture (99%), gene editing at this locus provided a system to study the *in vivo* gene editing efficacy of unoptimized and optimized LNPs after *in utero* IV administration. Thus, we administered PBS, A0 LNPs, or B5 LNPs *in utero* at a dose of 1 mg/kg total mRNA to E13.5 mouse fetuses. Mouse fetal livers were harvested after 5 d prior to isolation of genomic DNA and next-generation sequencing (NGS). Compared to A0 LNPs, B5 LNPs facilitated threefold greater insertions and deletions (indels) at the intended locus within the fetal liver (Fig. 5E). Thus, the B5 formulation for C14-490 LNPs was used as the basis for subsequent study of *in utero* gene editing in HSCs.

To demonstrate the proof-of-concept utility of our engineered platform for *in vivo* HSC gene editing therapies, we formulated C14-490 LNPs to encapsulate SpCas9 mRNA and TTR sgRNA using optimized B5 formulation parameters and surface conjugation to CD45 antibody F(ab')₂ fragments—Systematically optimized Targeted Editing Machinery LNPs (STEM LNPs). STEM LNPs, untargeted B5 LNPs, or PBS were administered IV at a dose of 1 mg/kg total mRNA to E13.5 wild-type mouse fetuses. After 5 d, mice were killed, and HSCs were isolated from the fetal liver or bone marrow via fluorescence-activated cell sorting (FACS). NGS demonstrated efficient editing (~6%) at the intended locus in genomic DNA isolated from the whole fetal liver of mice treated with either untargeted B5 LNPs or STEM LNPs (Fig. 5F). In contrast, fourfold higher levels of gene editing were observed at the intended locus in HSCs derived from the fetal liver (Fig. 5G) isolated from mice treated with STEM LNPs (~8%) relative to those from mice treated with untargeted LNPs (~2%). This relative improvement in gene editing was maintained in fetal HSCs that had already migrated into the bone marrow niche (*SI Appendix, Fig. S11*). Together, these results support the efficacy of our engineered STEM LNP platform in mediating gene editing of HSCs *in utero*.

Discussion

Ex vivo HSC-based gene therapies are increasingly being used for the treatment of monogenic blood diseases (33). However, the high cost and infrastructure requirements for these therapies can be limiting, especially for patients in under-resourced settings where these diseases are most prevalent (34). In addition, the myeloablative agents required for these therapies are not well-tolerated by some patients and have been associated with short- and long-term toxicity (9, 10). The pathology of many monogenic blood diseases begins before or shortly after birth and, as such, these diseases can be associated with significant childhood morbidity. At the extreme end of the spectrum, α thalassemia major can result in nonimmune fetal hydrops and fetal demise (1, 2). Thus, there is a need for a safe and effective *in vivo* approach to target hematopoietic progenitor cells before the onset of monogenic blood disease. Prior work from our group has demonstrated the feasibility of therapeutic *in utero* gene editing in mouse models of congenital diseases involving the liver, lung, and heart (35–37). In these studies, long-term genome correction of target tissues was achieved, suggesting that therapeutic genome editing had occurred in the progenitor cells of disease-relevant organs. To realize the potential of *in utero* gene editing therapies for monogenic blood disease, we engineered a targeted LNP platform designed to mediate *in vivo* gene editing of fetal HSCs without prior cytotoxic conditioning.

Our design approach leverages fetal and developmental biology to overcome conventional biological barriers in mRNA-LNP delivery to HSCs. Notably, residence of fetal hematopoiesis—and consequentially fetal HSCs—within the liver during development provides a more accessible compartment for LNP-mediated gene delivery in comparison to the postnatal bone marrow niche. Using a top-performing LNP from our prior study assessing the feasibility of *in utero* mRNA-LNP delivery to the fetal liver (26), we first demonstrated strong LNP-mediated transfection of the fetal liver at an early gestational age, as expected given intrinsic LNP hepatotropism, but low-level genome modification of fetal HSCs *in vivo*. To boost genome modification within fetal HSCs, we conjugated CD45 antibody F(ab')₂ fragments to the surface of these LNPs using thiol-maleimide chemistry. We hypothesized that targeted LNPs would engage the CD45R found expressed on the surface of hematopoietic cells residing in the fetal liver (21) and facilitate LNP internalization into these cells. Indeed, relative to untargeted LNPs, targeted LNPs enhanced mRNA delivery to hematopoietic lineage cells by eightfold *in vitro* and genome modification in HSCs by sevenfold *in vivo* following *in utero* IV administration to mid-gestation fetal mice without a preconditioning regimen.

Other groups have utilized CD117 (c-Kit) antibody fragments to target HSCs *in vivo* in adult recipients (19, 20). Although CD117 is a more specific HSC marker, its broad role in other developmental processes—including stemness in other organs and germline cell maturation (38)—made LNP conjugation to CD117 antibody fragments a less ideal approach for gene editing in the fetus. An alternative receptor to target for delivery to human HSCs is CD34, used widely to isolate human HSCs for *ex vivo* processing (33). However, the CD34 receptor is found on the surface of both HSCs and mesenchymal tissues in the developing human fetus and is not found on LT-HSCs in the mouse (39, 40). In contrast, the CD45 receptor has specificity to HSCs and their progeny, motivating selection of its cognate antibody for downstream LNP engineering. Interestingly, in our study, CD45R-targeted LNPs were unable to transfect bone marrow HSCs after IV administration in adult mice. We hypothesize that active targeting was unable to boost transfection efficacy in adult mice due to undetectable baseline transfection of bone marrow HSCs after IV administration of untargeted C14-490 LNPs to adult mice. Despite this limitation, the antibody conjugation approach utilized in this study is highly modular and could be used in combination with a range of base LNP formulations that may better passively traffic to the adult bone marrow. To target more specific immune cell populations, antibody fragments that target one or more desired cell surface receptors may be engineered. Some candidate congenital diseases that may benefit from more specific targeted LNP platforms include primary T cell (CD3, CD5, or CD7) or B cell (CD19) immunodeficiencies and leukodystrophies involving dysfunctional microglia in the brain (MRC1).

HSCs migrate from the fetal liver to the bone marrow late in development, where they reside and are responsible for definitive hematopoiesis (21). We hypothesized that HSCs edited via targeted LNPs within the fetal liver would naturally engraft in the bone marrow niche and produce myeloid and lymphoid progeny carrying the same edit during adult life. Encouragingly, after 4 mo, we observed that bone marrow HSCs of mice treated *in utero* with targeted LNPs possessed higher editing than mice treated *in utero* with untargeted LNPs. Although there was a reduction in the percentage of genome-edited HSCs at 4 mo relative to at 60 h, this may correspond to the initial transfection of both LT-HSCs and other types of hematopoietic progenitor cells with the latter populations not persisting to the 4mo time point. Encouragingly, when

we examined the peripheral blood of these cohorts of mice, hematopoietic lineage cells were transfected at the same proportion as their HSC progenitors. To better characterize the phenotype of transfected HSCs, we conducted a secondary transplant study that involved transferring donor HSCs 4 mo after modification in utero via targeted LNPs into irradiated recipients. Lethally irradiated wild-type mice were rescued by a bone marrow transplant from donor mice, and transfection of HSCs and hematopoietic lineage cells matched donor WBM transfection levels. Together, these data support that targeted LNPs robustly transfect self-renewing and multipotent populations of LT-HSCs without preconditioning at the time of fetal LNP injection.

Engineering cells in vivo during early development is not without potential risks. First, both the LNP platform and encapsulated gene editing cargo must not cause harm to the fetus, including not only through technical administration of the therapy but also through adverse effects of the therapeutic product itself. Second, the therapeutic gene target and editing strategy must be carefully selected to ensure that normal development is not disrupted by genome modification. Finally, as with all fetal interventions, genome editing must be confined to somatic cells given the complex ethical considerations involved in germline cell gene editing. In our study, targeted LNPs neither induced a significant acute cytokine response nor transaminitis, and fetal mice treated with targeted LNPs had a similar rate of survival to birth as PBS- and untargeted LNP-treated mice. While these data suggest that targeted LNPs have a similar safety profile to normal saline and untargeted LNPs and are generally safe for fetal mouse administration, further work is necessary to fully characterize the safety of the lead targeted LNP platform.

CRISPR-based gene editing strategies have the potential to revolutionize the treatment of congenital blood diseases, as exemplified by the recent approval of Casgevy™ and Lyfgenia™ for the treatment of sickle cell disease and transfusion-dependent β thalassemia (41). Fully realizing the potential of in vivo HSC gene editing therapies requires both reliable in vivo trafficking to HSCs and the codelivery of large genome editors (~4.5 kb) within the delivery vector. However, there has been limited success in demonstrating strong in vivo transfection of HSCs, despite viral capsid engineering and optimization of existing nanocarriers. In addition, although there are promising efforts to reduce the size of genome editors or split them across vectors (42), the delivery of large genome editing cargo in vivo to HSCs remains a challenge. Here, by using high-throughput DOE to investigate a large ($4 \times 4 \times 4 \times 4$) design space of LNP formulations, we identified a set of LNP formulation parameters optimized for the codelivery of SpCas9 mRNA and sgRNA. The lead B5 formulation resulted in tenfold improvement in gene knockout in hematopoietic lineage cells in vitro and threefold greater indels at the proof-of-concept *TTR* locus in the whole fetal liver in vivo. Combining the optimized LNP formulation with our CD45 targeting strategy resulted in STEM LNPs, a platform engineered specifically for gene editing fetal HSCs. Upon in utero IV administration, STEM LNPs facilitated equivalent gene editing in the whole fetal liver and fourfold greater indels at the *TTR* locus in fetal HSCs in comparison to untargeted LNPs. Extending these results more broadly, substitution of the editing cargo within STEM LNPs for disease-specific sgRNAs could produce in vivo therapeutic strategies for a range of congenital hematopoietic disorders, including hemoglobinopathies, immunodeficiencies, leukodystrophies, and lysosomal storage diseases.

Materials and Methods

Ionizable Lipid Synthesis. C14-490 ionizable lipids were synthesized as previously described (43). Briefly, 3-(4-{2-[(3-amino-2-ethoxypropyl)amino]ethyl})

piperazin-1-yl)-2-ethoxypropan-1-amine (denoted as 490, Enamine, Kyiv, Ukraine) was combined with excess 1,2 epoxytetradecane (denoted as C14, MilliporeSigma, Burlington, MA) in a 4 mL glass scintillation vial with a magnetic stir bar for 2 d at 80 °C. The reaction product was transferred to a Rotovapor R-300 for solvent evaporation. To purify this product, lipid fractions were separated via a CombiFlash Nextgen 300+ chromatography system (Teledyn ISCO, Lincoln, NE). The fraction containing C14-490 ionizable lipid was identified via liquid chromatography-mass spectrometry (LC-MS). C14-490 ionizable lipid was suspended in ethanol for downstream use.

mRNA Production. GFP, mCherry, and Cre recombinase mRNA was sourced from TriLink Biotechnologies (San Diego, CA) with CleanCap® modifications. CRISPRRevolution™ sgRNAs were sourced from Synthego (Redwood City, CA). The sequence for GFP sgRNA was 5′-GGGCGAGGAGCUGUACCCG-3′, while the sequence for TTR sgRNA was 5′-UUACAGCCAGCUCUACAGCA-3′.

SpCas9 mRNA was produced using standard in vitro transcription methods. In brief, the SpCas9 gene sequence was codon optimized, synthesized, and cloned into proprietary mRNA production plasmids. The m¹Ψ UTP nucleoside-modified mRNA was cotranscriptionally capped with a trinucleotide cap1 analogue (TriLink, San Diego, CA) and engineered to contain a 101 nucleotide-long poly(A) tail. Transcription was performed using MegaScript T7 RNA polymerase (Invitrogen, Waltham, MA), and mRNA was purified by fast protein liquid chromatography using an Akta Purifier (GE Healthcare, Chicago, IL). mRNA product integrity was validated using agarose gel electrophoresis and mRNA was stored frozen at -80 °C for later use.

LNP Formulation and Characterization. C14-490 ionizable lipid was combined in ethanol with cholesterol (MilliporeSigma), 1,2-dioleoyl-*sn*-glycero-3-phosphoethanolamine (DOPE, Avanti Polar Lipids, Alabaster, AL), and 1,2-dimyristoyl-*sn*-glycero-3-phosphoethanolamine-N-[methoxy(polyethylene glycol)-2000] (C14-PEG2000, Avanti Polar Lipids) to a total volume of 112.5 μ L at a molar ratio of 35:46.5:16:2.5 to produce C14-490 LNPs. For untargeted and targeted LNPs, a 5:1 ratio of C14-PEG2000 to 1,2-distearoyl-*sn*-glycero-3-phosphoethanolamine (DSPE)-anchored PEG-maleimide (Avanti Polar Lipids) was used at the same molar ratio. For DOE optimization of C14-490 LNP formulation, the molar ratios were derived from the design tables found in *SI Appendix, Figs. S8 and S10*. A separate aqueous phase was prepared from 25 μ g of GFP mRNA, mCherry mRNA, Cre mRNA, or a combination of SpCas9 mRNA and GFP or TTR sgRNA (4:1 mass ratio) in 10 mM citrate buffer to a total volume of 337.5 μ L. The ethanol and aqueous phases were combined via chaotic mixing using a herringbone microfluidic device to produce LNPs. LNPs were dialyzed against 1 \times PBS in Slide-A-Lyzer G2 20 kDa dialysis cassettes (Thermo Fisher Scientific) for 2 h, sterilized using 0.22 μ m filters, and stored at 4 °C for future use.

For preparation of targeted LNPs, anti-mouse CD45.2 antibodies (Biolegend, San Diego, CA), anti-human (BC8) CD45 antibodies (Thermo Fisher Scientific), or IgG isotype control (IgG1, κ) antibodies (Biolegend) were first cut into F(ab)₂ fragments using either IdeZ enzymes (mouse, New England Biolabs, Ipswich, MA) or ficin enzymes (human, Thermo Fischer Scientific) via manufacturer specifications. Antibody fragments were then reduced via dithiothreitol (DTT) for 30 min at 25 °C. DTT was removed using centrifugation through a 10 kDa filter (MilliporeSigma), and the antibody product was resuspended in 1 \times PBS. Targeted LNPs were generated via reaction of untargeted LNPs to an excess of generated F(ab)₂ fragments for 1 h at room temperature followed by overnight incubation at 4 °C. Free antibody fragments were removed through column filtration using Sephadex G-75 beads (MilliporeSigma). Targeted LNPs were subsequently concentrated using 50 kDa Amicon Ultra-2 Centrifugal Filter Units (Sigma Aldrich) prior to use.

Zetasizer Nano (Malvern Instruments, Malvern, UK) was used to measure the z-average diameter and polydispersity index (PDI) of LNPs. Encapsulation efficiency was measured using a Quant-iT-RiboGreen (Thermo Fisher Scientific) assay via manufacturer specifications. All LNP characterization data were reported as the mean of triplicate measurements. All materials were prepared and handled nuclease-free throughout synthesis, formulation, and characterization steps.

In Vitro Assessment of Targeted LNPs. For testing the efficacy of CD45-conjugation to LNPs, Jurkat cells were seeded at a density of 30,000 cells/100 μ L in serum-free media (OptiMem, Thermo Fisher Scientific) and treated with untargeted LNPs or targeted LNPs encapsulating GFP mRNA at a dose of 100 ng total mRNA, unless otherwise specified. After 24 h, cells were harvested, resuspended

in flow cytometry buffer ($\text{Ca}^{2+}/\text{Mg}^{2+}$ Free PBS, 0.5% BSA, 0.5 mM EDTA), and analyzed via flow cytometry for GFP fluorescence. Viability of treated Jurkat cells was assessed via Live/Dead™ Cytotoxicity Kit (Thermo Fisher Scientific).

For studies investigating the specificity of CD45-conjugation to LNPs, Jurkat cells were seeded at a density of 30,000/100 μL and then treated with either free anti-human (BC8) CD45 antibody (Thermo Fisher Scientific) or free IgG isotype control (IgG1, κ) antibody (Biolegend) at a range of doses. After 30 min, untargeted LNPs or targeted LNPs encapsulating GFP mRNA at a dose of 100 ng total mRNA were added to the media. After 24 h, cells were harvested, resuspended in flow cytometry buffer, and analyzed via flow cytometry for GFP fluorescence. In an additional experiment, HepG2 cells were seeded at a density of 20,000/100 μL and then treated with untargeted LNPs or targeted LNPs encapsulating GFP mRNA at a dose of 25 ng. After 24 h, cells were harvested, resuspended in flow cytometry buffer, and analyzed via flow cytometry for GFP fluorescence.

For studies assessing the impact of the protein corona on LNP delivery, Jurkat cells were seeded at a density of 30,000/100 μL . Untargeted LNPs or targeted LNPs encapsulating GFP mRNA were incubated at 37 °C for 15 min in PBS or purified mouse plasma at a 1:1 volume ratio. Each suspension was used to treat Jurkat cells at a dose of 100 ng total mRNA. After 24 h, cells were harvested, resuspended in flow cytometry buffer, and analyzed for GFP+ via flow cytometry.

LNP Protein Corona Characterization. Either untargeted or targeted LNPs encapsulating GFP mRNA were prepared in quadruplicate as described previously in this section. Purified mouse plasma (EDTA) was added to each LNP solution at a 1:1 volume ratio and incubated at 37 °C for 15 min. The LNP/plasma mixture was subsequently loaded onto a 0.7-M sucrose cushion of equal volume to the mixture and centrifuged at 15,300 g at 4 °C for 1 h. The resultant protein pellet was washed with 1× PBS prior to submission to the Children's Hospital of Philadelphia-Penn Proteomics Core for mass spectrometry analysis.

Animals. All animal use and protocols were approved by the Institutional Animal Care and Use Committee (IACUC) at the Children's Hospital of Philadelphia and followed guidelines of the NIH's Guide for the Care and Use of Laboratory Animals. BALB/c (stock #000651), C57BL/6J (#000664), and B6.129(Cg)-Gt(ROSA)26Sor^{tm4(ACTB-tdTomato,-EGFP)Lox/J} ($R26^{\text{m/mG}}$, stock #007676) were purchased from The Jackson Laboratory (Bar Harbor, ME). Mice were housed in the Laboratory Animal Facility of the Colket Translational Research Building at the Children's Hospital of Philadelphia.

In Utero and Adult Mouse IV Injection. Fetuses of time-dated pregnant mice were injected at E13.5 as previously described (35). Briefly, under isoflurane anesthesia, a midline laparotomy was performed to expose the uterine horns. Under a dissecting microscope, the vitelline vein of each fetus was identified, and a total volume of 5 μL was injected using an 80- μm beveled glass micropipette and an automated microinjector (Narishige International USA Inc., Amityville, NY). Successful injection was confirmed by clearance of blood in the vein by the injectate. Subsequently, the uterus was returned to the peritoneal cavity, and the abdomen was closed with a single layer of absorbable 4-0 polyglactin 910 suture. For studies in adult mice (12 wk old), IV administration was performed via standard access of the lateral tail vein (24).

Fetal Mouse Histology. Untargeted or targeted LNPs encapsulating mCherry mRNA were administered via in utero IV injection at a dose of 1 mg/kg to E13.5 Balb/c mouse fetuses. After 24 h, whole mouse fetuses were harvested and fixed in 4% paraformaldehyde (PFA) overnight at 4 °C prior to dehydration in alcohol and paraffin embedding. Tissue sections were dewaxed and rehydrated through xylene and ethanol treatment prior to immunofluorescence processing. For immunodetection, 10 mM citrate buffer (pH 6) was used for antigen retrieval, and sections were blocked with 10% donkey serum in 1% BSA prior to primary antibody (beta-3 tubulin, alpha-smooth muscle actin, CD31, CD45) incubation overnight at 4 °C. Fluorescence-conjugated Alexa Fluor secondary antibodies were used (Invitrogen, Carlsbad, CA) according to the primary antibody species and counterstained with DAPI. Sections were mounted on slides, and images were collected via a Zeiss LSM 880 confocal microscope.

In Vivo Analysis of LNP Genome Modulation. To establish baseline LNP transfection of fetal HSCs, PBS or C14-490 LNPs encapsulating Cre mRNA was administered IV to E13.5 fetal $R26^{\text{m/mG}}$ mice. Transfection of the whole fetus and fetal liver

was assessed via stereomicroscopy and percentage of GFP+ in fetal hepatocytes (CD45-/CD31-) and fetal HSCs (Lin-/Sca1+/cKit+) via flow cytometry.

To assess in vivo efficacy of untargeted and targeted LNPs, untargeted LNPs or targeted LNPs encapsulating Cre mRNA were administered IV to either E13.5 fetal $R26^{\text{m/mG}}$ mice or 12-wk-old adult $R26^{\text{m/mG}}$ mice. For short-term studies (60 h), fetal liver was processed to assess transfection of fetal hepatocytes (CD45-/CD31-) and fetal HSCs (Lin-/Sca1+/cKit+) via flow cytometry, while adult liver and bone marrow were processed to assess transfection of adult hepatocytes (CD45-/CD31-) and adult HSCs (Lin-/Sca1+/cKit+). For long-term studies (4 mo), adult liver and bone marrow were processed for both groups. Prior to terminal harvest of mice treated as fetuses, a multilineage analysis of peripheral blood was performed to determine transfection of T cells (CD3+), B cells (B220+), monocytes (Cd11b+), granulocytes (Gr1+), and erythrocytes (Ter119+).

In Vivo Safety Studies. To assess liver toxicity, blood samples were collected 24 h after injection of PBS, untargeted LNPs, or targeted LNPs in E13.5 $R26^{\text{m/mG}}$ mice. Fetal plasma was isolated via centrifugation and AST, ALT, and alkaline phosphatase levels were subsequently assessed via a Roche Cobas Chemistry Analyzer (Roche, Basel, Switzerland). For cytokine analysis, blood samples were collected 24 h or 48 h after injection of PBS, untargeted LNPs, or targeted LNPs in E13.5 $R26^{\text{m/mG}}$ mice. Fetal serum was isolated via centrifugation and analyzed via a 25-proinflammatory cytokine panel (MilliporeSigma) or Mouse GM-CSF DuoSet ELISA (R&D Systems, Minneapolis, MN) according to the manufacturer's instructions. Multiplex plates were run on a MAGPIX® system (Luminex Corporation, Austin, TX) with a minimum of 50 beads analyzed per region. Each cytokine was assessed using a five-parameter regression algorithm and normalized to the protein concentration in the sample.

Secondary Transplant Study. Targeted LNPs encapsulating Cre mRNA at a dose of 1 mg/kg were administered to E13.5 $R26^{\text{m/mG}}$ mouse fetuses via in utero IV injection. After 16 wk, WBM was harvested from mice (donors). In brief, tibias, femurs, and iliac bones were flushed with sterile PBS prior to filtration and layering over Ficoll-Paque PLUS (GE Healthcare) to isolate a low-density mononuclear cell layer. After cells were counted, a sample of WBM was analyzed for fluorescence (GFP+) via flow cytometry to determine donor cell transfection. C57/BL6 × Balb/c F1 mice (12 wk old, recipient) were lethally irradiated (10.4 Gy, split between two doses) prior to transplantation of isolated donor WBM (750,000 cells). Recipient mice were followed for 4 mo via monthly peripheral blood draws prior to terminal bone marrow harvest. At terminal harvest, a multilineage analysis of peripheral blood was performed to determine transfection of T cells (CD3+), B cells (B220+), monocytes (Cd11b+), granulocytes (Gr1+), and erythrocytes (Ter119+). In addition, transfection of donor HSCs engrafted in recipient bone marrow was assessed by isolation of WBM and flow cytometric analysis of GFP fluorescence in HSCs (Lin-/Sca1+/cKit+).

In Vitro DOE Screen of LNP Formulations. For DOEs, HepG2-GFP or Jurkat-GFP cells were cultured in Dulbecco's Modified Eagle's Medium with L-glutamine (Gibco, Dublin, Ireland) or Roswell Park Memorial Institute 1,640 media supplemented with 10% volume/volume of fetal bovine serum (Gibco) and 1% volume/volume penicillin-streptomycin (Gibco). HepG2-GFP cells were seeded at a density of 20,000 cells/100 μL , while Jurkat-GFP cells were seeded at a density of 30,000 cells/100 μL . LNPs containing a total of 150 ng total mRNA were used to treat cells, media was exchanged after 24 h, and cells were grown for a total of 5 d. At harvest, cells were isolated and resuspended in flow cytometry buffer ($\text{Ca}^{2+}/\text{Mg}^{2+}$ Free PBS, 0.5% BSA, 0.5 mM EDTA). Samples were analyzed for fluorescence (GFP+) via flow cytometry (BD FACSAria™ Cell Sorter, Haryana, India). Viability was assessed in a duplicate plate of treated cells via Live/Dead™ Cytotoxicity Kit (Thermo Fisher Scientific).

Isolation of Genomic DNA and NGS. STEM LNPs, untargeted B5 LNPs, or PBS were administered via in utero IV injection at a dose of 1 mg/kg total mRNA to E13.5 Balb/c mouse fetuses. After 5 d, tissues were harvested and genomic DNA of fetal liver or fetal HSCs, isolated via FACS (Lin-/Sca1+/cKit+), was extracted using a DNEasy Blood and Tissue Kit according to the manufacturer's instructions (Qiagen, Hilden, Germany). PCR amplification of the target amplicon was carried out using SuperFi II Hi-Fidelity DNA Polymerase (Thermo Fisher Scientific) with a universal annealing temperature of 60 °C and the following primer sequences: mTTR-exon2-F, 5'-CGGTTACTCTGACCCATTC-3', and mTTR-exon2-R,

5'-GGGCTTCTACAAGCTTACC-3'. Full-length Illumina sequencing adapters were then added to PCR products using a Nextera XT DNA Library Preparation Kit (Illumina, San Diego, CA). Pooled samples were sequenced using an Illumina MiSeq system. Alignment of fastq files to the target amplicon and quantification of editing frequency at the *TTR* locus was performed using CRISPResso2.

Statistical Analysis. All statistical analyses were carried out using GraphPad Prism 8 software. As described in figure captions, unpaired Student's *t* tests, one-way ANOVA with post hoc Dunnett's test, or two-way ANOVA with post hoc Sidák's multiple comparisons test were used to determine significance.

Data, Materials, and Software Availability. All study data, materials and methods, and software are included in the article, *SI Appendix*, or cited appropriately.

ACKNOWLEDGMENTS. We acknowledge the Children's Hospital of Philadelphia Translational Research Core and the Children's Hospital of Philadelphia-Penn Proteomics Core for their assistance with this project. Figure schematics were

created with the use of BioRender. This study was supported by the U.S. NIH Director's New Innovator Awards (DP2TR002776 to M.J.M. and DP2HL152427 to W.H.P.) and NIH R01DK123049 (awarded to M.J.M. and W.H.P.). R.P. was supported by an NIH National Heart, Lung, and Blood Institute Ruth L. Kirschstein Pre-Doctoral National Research Service Award (F30HL162465-01A1).

Author affiliations: ^aDepartment of Bioengineering, University of Pennsylvania, Philadelphia, PA 19104; ^bCenter for Fetal Research, Division of General, Thoracic, and Fetal Surgery, Children's Hospital of Philadelphia, Philadelphia, PA 19104; ^cDepartment of Medicine, Perelman School of Medicine, University of Pennsylvania, Philadelphia, PA 19104; ^dDepartment of Psychiatry, Perelman School of Medicine, University of Pennsylvania, Philadelphia, PA 19104; and ^eDepartment of Pathology, Perelman School of Medicine, University of Pennsylvania, Philadelphia, PA 19104

Author contributions: R.P., J.S.R., S.K.B., M.J.M., and W.H.P. designed research; R.P., J.S.R., S.K.B., V.L., A.D., N.K., B.M.W., A.S.R., K.S., L.X., D.S., A.S.T., H.S., V.S.C., M.C., E.L.H., R.M., A.G.H., K.M., and M.B.B. performed research; P.W.Z., M.-G.A., and D.W. contributed new reagents/analytic tools; R.P., M.J.M., and W.H.P. analyzed data; and R.P., M.J.M., and W.H.P. wrote the paper.

1. E. Kohne, Hemoglobinopathies. *Dtsch. Arztebl. Int.* **108**, 532-540 (2011).
2. C. L. Harteveld *et al.*, The hemoglobinopathies, molecular disease mechanisms and diagnostics. *Int. J. Lab. Hematol.* **44**, 28-36 (2022).
3. D. H. K. Chui, J. S. Waye, Hydrops fetalis caused by α -thalassemia: An emerging health care problem. *Blood* **91**, 2213-2222 (1998).
4. R. Palanki, W. H. Peranteau, M. J. Mitchell, Delivery technologies for in utero gene therapy. *Adv. Drug Deliv. Rev.* **169**, 51 (2021).
5. V. Prakash, M. Moore, R. J. Yáñez-Muñoz, Current progress in therapeutic gene editing for monogenic diseases. *Mol. Ther.* **24**, 465-474 (2016).
6. H. Frangoul *et al.*, CRISPR-Cas9 gene editing for sickle cell disease and β -thalassemia. *N. Engl. J. Med.* **384**, 252-260 (2021).
7. G. Ferrari, A. J. Thrasher, A. Aiuti, Gene therapy using haematopoietic stem and progenitor cells. *Nat. Rev. Genet.* **22**, 216-234 (2021).
8. C. Sheridan, The world's first CRISPR therapy is approved: Who will receive it? *Nat. Biotechnol.* **42**, 3-4 (2023), 10.1038/d41587-023-00016-6.
9. S. Bhatia, Long-term health impacts of hematopoietic stem cell transplantation inform recommendations for follow-up. *Expert Rev. Hematol.* **4**, 437-454 (2011).
10. D. Buchbinder *et al.*, Neurocognitive dysfunction in hematopoietic cell transplant recipients: Expert review from the late effects and quality of life working committee of the CIBMTR and complications and quality of life working party of the EBMT. *Bone Marrow Transplant.* **53**, 535-555 (2018).
11. K. Cornetta *et al.*, Gene therapy access: Global challenges, opportunities, and views from Brazil, South Africa, and India. *Mol. Ther.* **30**, 2122-2129 (2022).
12. D. B. Kohn, Gene therapy for blood diseases. *Curr. Opin. Biotechnol.* **60**, 39-45 (2019).
13. S. K. Bose, P. Menon, W. H. Peranteau, In utero gene therapy: Progress and challenges. *Trends Mol. Med.* **27**, 728-730 (2021).
14. C. Li *et al.*, In vivo HSC gene therapy using a Bi-modular HDAd5/35++ vector cures sickle cell disease in a mouse model. *Mol. Ther.* **29**, 822 (2021).
15. C. Li *et al.*, In vivo HSC prime editing rescues sickle cell disease in a mouse model. *Blood* **141**, 2085-2099 (2023).
16. J. T. Bulcha, Y. Wang, H. Ma, P. W. L. Tai, G. Gao, Viral vector platforms within the gene therapy landscape. *Signal Transduct. Target Ther.* **6**, 1-24 (2021).
17. X. Han *et al.*, An ionizable lipid toolbox for RNA delivery. *Nat. Commun.* **12**, 7233 (2021).
18. J. Kim, Y. Eygeris, R. C. Ryals, A. Jozic, G. Sahay, Strategies for non-viral vectors targeting organs beyond the liver. *Nat. Nanotechnol.* **19**, 428-447 (2023), 10.1038/s41565-023-01563-4.
19. D. Shi, S. Toyonaga, D. G. Anderson, In vivo RNA delivery to hematopoietic stem and progenitor cells via targeted lipid nanoparticles. *Nano Lett.* **23**, 2938-2944 (2023).
20. L. Breda *et al.*, In vivo hematopoietic stem cell modification by mRNA delivery. *Science* **381**, 436-443 (2023).
21. K. Lewis, M. Yoshimoto, T. Takebe, Fetal liver hematopoiesis: From development to delivery. *Stem Cell Res. Ther.* **12**, 139 (2021).
22. K. L. Swingle, A. G. Hamilton, M. J. Mitchell, Lipid nanoparticle-mediated delivery of mRNA therapeutics and vaccines. *Trends Mol. Med.* **27**, 616-617 (2021).
23. M. M. Billingsley *et al.*, Orthogonal design of experiments for optimization of lipid nanoparticles for mRNA engineering of CAR⁺ cells. *Nano Lett.* **22**, 533-542 (2022).
24. H. C. Safford *et al.*, Orthogonal design of experiments for engineering of lipid nanoparticles for mRNA delivery to the placenta. *Small*, 10.1002/smll.202303568 (2023).
25. T. Wei *et al.*, Delivery of tissue-targeted scalpels: Opportunities and challenges for in vivo CRISPR/Cas-based genome editing. *ACS Nano* **14**, 9243-9262 (2020).
26. R. S. Riley *et al.*, Ionizable lipid nanoparticles for in utero mRNA delivery. *Sci. Adv.* **7**, eaba1028 (2021).
27. S. L. McKinney-Freeman *et al.*, Surface antigen phenotypes of hematopoietic stem cells from embryos and murine embryonic stem cells. *Blood* **114**, 268-278 (2009).
28. R. Palanki *et al.*, Ionizable lipid nanoparticles for therapeutic base editing of congenital brain disease. *ACS Nano* **17**, 13594-13610 (2023).
29. A. C. Wilkinson, K. J. Igarashi, H. Nakauchi, Haematopoietic stem cell self-renewal in vivo and ex vivo. *Nat. Rev. Genet.* **21**, 541-554 (2020).
30. A. G. Hamilton, K. L. Swingle, M. J. Mitchell, Biotechnology: Overcoming biological barriers to nucleic acid delivery using lipid nanoparticles. *PLoS Biol.* **21**, e3002105 (2023).
31. K. J. Kauffman *et al.*, Optimization of lipid nanoparticle formulations for mRNA delivery in vivo with fractional factorial and definitive screening designs. *Nano Lett.* **15**, 7300-7306 (2015).
32. J. D. Finn *et al.*, A single administration of CRISPR/Cas9 lipid nanoparticles achieves robust and persistent in vivo genome editing. *Cell Rep.* **22**, 2227-2235 (2018).
33. E. Zonari *et al.*, Efficient ex vivo engineering and expansion of highly purified human hematopoietic stem and progenitor cell populations for gene therapy. *Stem Cell Rep.* **8**, 977-990 (2017).
34. B. Johnson, Reducing the costs of blockbuster gene and cell therapies in the Global South. *Nat. Biotechnol.* **42**, 8-12 (2024), 10.1038/s41587-023-02049-3.
35. A. C. Rossidis *et al.*, In utero CRISPR-mediated therapeutic editing of metabolic genes. *Nat. Med.* **24**, 1513-1518 (2018).
36. D. Alapati *et al.*, In utero gene editing for monogenic lung disease. *Sci. Transl. Med.* **11**, eaav8375 (2019).
37. S. K. Bose *et al.*, In utero adenine base editing corrects multi-organ pathology in a lethal lysosomal storage disease. *Nat. Commun.* **12**, 4291 (2021).
38. M. Miettinen, J. Lasota, KIT (CD117): A review on expression in normal and neoplastic tissues, and mutations and their clinicopathologic correlation. *Appl. Immunohistochem. Mol. Morphol.* **13**, 205 (2005).
39. C. Viswanathan, R. Kulkarni, A. Bopardikar, S. Ramdasi, Significance of CD34 negative hematopoietic stem cells and CD34 positive mesenchymal stem cells—A valuable dimension to the current understanding. *Curr. Stem Cell Res. Ther.* **12**, 476-483 (2017).
40. G. A. Challen, N. Boles, K. K. Lin, M. A. Goodell, Mouse hematopoietic stem cell identification and analysis. *Cytometry A* **75**, 14-24 (2009).
41. E. Harris, Sickle cell disease approvals include first CRISPR gene editing therapy. *JAMA* **331**, 280 (2024), 10.1001/jama.2023.26113.
42. A. Raguram, S. Banskota, D. R. Liu, Therapeutic in vivo delivery of gene editing agents. *Cell* **185**, 2806-2827 (2022).
43. K. T. Love *et al.*, Lipid-like materials for low-dose, in vivo gene silencing. *Proc. Natl. Acad. Sci. U.S.A.* **107**, 1864-1869 (2010).